Local Adjustment of the Background Error Correlation for Surface Analyses over Complex Terrain

David T. Myrick[1] and John D. Horel
NOAA/Cooperative Institute for Regional Prediction and
Department of Meteorology, University of Utah
Salt Lake City, UT

Steven M. Lazarus
Florida Institute of Technology
Melbourne, FL

---

1. Corresponding author address:
University of Utah
Department of Meteorology
135 South 1460 East, Rm. 819
Salt Lake City, UT 84112-0110
email: dmyrick@met.utah.edu

Abstract

The terrain between gridpoints is used to modify locally the background error correlation matrix in an objective analysis system. This modification helps to reduce the influence across mountain barriers of corrections to the background field that are derived from surface observations. This change to the background error correlation matrix is tested using an analytic case of surface temperature that encapsulates the significant features of nocturnal radiation inversions in mountain basins, which can be difficult to analyze because of locally sharp gradients in temperature. Bratseth successive corrections, optimal interpolation, and three-dimensional variational approaches are shown to yield exactly the same surface temperature analysis. Adding the intervening terrain term to the Bratseth approach leads to solutions that match more closely the specified analytic solution. In addition, the convergence of the Bratseth solutions to the best linear unbiased estimation of the analytic solution is faster.

The intervening terrain term was evaluated in analyses over the western United States derived from a modified version of the Advanced Regional Prediction System Data Assimilation System. Local adjustment of the background error correlation matrix led to improved surface temperature analyses by limiting the influence of observations in mountain valleys that may differ from the weather conditions present in adjacent valleys.

1. Introduction

Accurate objective analyses of meteorological quantities are of great importance to weather forecasters. The need for analyses of meteorological surface variables (temperature, wind, etc.) over mountainous regions for applications such as forest fire suppression, winter road maintenance, and dispersion of pollutants in urban basins is receiving increasing attention (Smith et al. 1997). These applications require surface analyses at high spatial resolution (order 1-5 km).

As described by Lazarus et al. (2002), objective analyses of surface weather variables in the western United States are being generated at high spatial resolution using a revised version of the Advanced Regional Prediction System Data Assimilation System (ADAS; Brewster 1996; Xue et al. 2000, 2001, 2003). For the objective analysis, ADAS employs the Bratseth method of successive corrections (Bratseth 1986). This method was chosen over more advanced variational schemes employed by the operational centers because it is an inexpensive analysis procedure that can be run in near real-time over a large horizontal domain at high horizontal resolution. The Bratseth method has been shown to converge to the best linear unbiased estimation of the unknown truth (Bratseth 1986; Daley 1991; Kalnay 2003).

Many successive corrections, optimal interpolation, and variational analysis methods assume that observation corrections or innovations (differences between observations and the background) are weighted only as a function of the distance between the observation locations and grid points. This homogeneous assumption follows directly from the specification that the correlation between the background errors for any pair of gridpoints is independent of location (Kalnay 2003). The irregular distribution of observations in the horizontal and vertical complicates objective analyses of surface variables when the background error correlation matrix is specified a priori, particularly over complex terrain where the majority of the observations are

located in populated valleys. If the observations are relatively error free and their density is uniformly high throughout the analysis domain, the analysis should be constrained tightly by the observations. In this best case scenario, the resulting analysis should be able to resolve small-scale features, such as local mountain-valley circulations. However, when the data density is irregular (i.e., some subregions with high density and others with low density), the desire to resolve the local microclimate of one region may conflict with the need to spread the influence of observations into nearby data void regions.

Under certain meteorological conditions (e.g., cold air confined to one side of a mountain range or radiation inversions in mountain valleys), observational corrections on one side of a range can be quite different from those on the other side at similar elevations. If the background errors in the analysis scheme are specified to be strongly correlated across the range, then the differing observational increments may lead to a poor analysis, e.g., during a cold air damming event with cold air to the east of a range, the analysis on the east (west) side will tend to be too warm (cold). Such analysis errors could be reduced by using computationally expensive approaches (e.g., ensemble Kalman filters) that estimate rather than specify the background error correlation matrix (Kalnay 2003). In the context of less expensive analysis approaches, these errors could also be reduced by specifying a shorter background error correlation length scale so that the corrections are given negligible weight across the range. However, the variable width of the terrain in the western United States complicates the selection of a single representative length scale. An alternative approach involves using the terrain to restrict locally the length scale of the background error correlation.

Such local (anisotropic) weighting approaches have been proposed as a solution to various problems in the field of meteorological objective analysis in the past. Endlich and Mancuso

(1968) and Sasaki (1971) improved wind analyses by modifying a successive corrections scheme so that greater weight was given to upwind and downwind observations compared to those in crosswind directions. Thiebaux (1976, 1977) introduced an anisotropic correlation function that improved analyses of height fields. Hessler (1984) improved analyses of surface temperature in a coastal zone by weighting spatial covariances based upon proximity to the coastline. Benjamin and Seaman (1985) tested elliptical and banana-shaped weighting functions on a curved flow field. Lazinger and Steinacker (1990) modified the observational error covariances for station pairs on opposite sides of the Alps to account for the observed sharp gradients in isentropic surfaces across the range. Miller and Benjamin (1992) describe how anisotropic functions are used to analyze potential temperature, wind and humidity in the Mesoscale Analysis and Prediction System. Otte et al. (2001) introduced synoptic-dependent anisotropic weights into the Pennsylvania State University-National Center for Atmospheric Research Mesoscale Model that increased forecast skill. Benjamin et al. (2004a, 2004b) describe how static stability is used in the Rapid Update Cycle to determine the vertical influence of observations. Deng and Stull (2004) have proposed an analysis strategy designed especially for narrow, serpentine mountain valleys. Their relatively computationally expensive approach allows the background error correlation between two locations within the same valley to remain high, even if they are separated in a direct line by a ridge.

The primary objective of this research is to improve objective analysis methods for use in the western United States. The specific approach to be evaluated is a modification to the specification of the background error correlation used in the Bratseth successive corrections method such that observational innovations to the background field receive less weight when the locations of the observations and grid points are separated by mountain ranges. This approach involves searching for a barrier between observation and grid point pairs. If higher terrain is found to block the

path between the two points, then the influence of the observational increment upon the background field will be decreased. Our premise is that in the absence of local observations, the analysis should remain close to the background.

An analytic example will be used in section 2 to help motivate the need to modify the objective analysis scheme used by ADAS as well as demonstrate some of the characteristics of the resulting solutions. Modifications made to the University of Utah version of ADAS are described in section 3. In section 4, a case study is presented that illustrates the sensitivity of the ADAS analyses to the intervening terrain term. Conclusions and future work are discussed in section 5.

2. Motivation and Example

To help motivate why the background error correlations used in ADAS need to be modified locally for surface analyses over the western United States, we present an idealized case of a common weather phenomenon in northern Utah, a strong nocturnal radiation inversion in a valley. The terrain over northern Utah is shown in Fig. 1. Our focus is along line segment AB in Fig. 1, which cuts across the Rush Valley, through the Oquirrh Mountains, and across the Salt Lake Valley. The eastern slopes of the Salt Lake and Rush Valleys are herein referred to as benches (see Fig. 1). As will be shown in Section 4, the temperature near the floor of the Rush Valley is often much colder than that along the floor of the Salt Lake Valley when strong radiation inversions develop. In addition, the surface temperature profile in both valleys becomes inverted with higher temperatures on the benches. The large temperature gradients that develop over short distances within the valleys as well as the differences in the temperature structure between nearby valleys are difficult to analyze objectively, especially since the background fields obtained by operational

6

and research models do not usually resolve adequately the horizontal and vertical thermodynamic structure of the nocturnal boundary layer found in such basins (Doran et al. 2002).

The terrain profile along the line AB in Fig. 1 is idealized by sinusoidal functions as shown in Fig. 2 such that the Rush Valley is approximately 300 m higher in elevation than the Salt Lake Valley and the idealized Oquirrh Mountains rise roughly 1 km above the valley sidewalls (the latter of which are hereafter referred to as benches). An idealized radiation inversion, represented by an analytic temperature profile (at 1-km resolution), is shown by the line labeled "truth" in Fig. 2. In this example, temperatures near the floor of the Rush Valley are specified to be 2°C colder than those on the adjacent benches and those over the floor of the Salt Lake Valley. A less pronounced temperature inversion is specified in the Salt Lake Valley.

A sample of 500 analyses was created using observations at the 10 locations indicated by filled circles along the terrain profile in Fig. 2. This distribution of observations crudely reflects the typical spacing of observations in the area with four stations located in the Rush Valley, one near the crest of the Oquirrhs, and five in the Salt Lake Valley. The observations are unbiased (i.e., the sample average of the observations indicated by the open boxes in Fig. 2 equals truth) with the sample variance of the random observational errors at each location set to 0.1°C. In this idealized setting, 500 background fields are specified with both random and systematic errors such that on average the background fields are significantly warmer than truth on the valley floors and the crest of the Oquirrhs, unbiased near specific locations on the slopes (3, 29, 34, 46, 60, and 91 km), and too cold on the benches (Fig. 2).

Dee and da Silva (1998) define an approach to mitigate the impact of systematic errors of the background field. However, since the background fields are not likely to have the same biases during other times of the day and other synoptic situations, we prefer to assume that the back-

ground field is unbiased. This assumption, combined with the large background bias errors evident in Fig. 2, leads to distinct background error correlations that vary as a function of location (not shown). For example, errors in the core of the Rush and Salt Lake Valleys are strongly related to one another and are inversely related to errors on the nearby benches and upper slopes. In addition, the errors on the benches are related strongly to those on the other benches over the entire width of the domain. Hence, the correlation between the background errors do not simply decrease isotropically with distance.

Objective analysis systems often do assume that the background error correlation decreases with increasing horizontal and vertical distance, e.g.,

$$\rho_{ij} = \exp\left(\frac{-\left|r_{ij}\right|^2}{R^2}\right)\exp\left(\frac{-\left|z_{ij}\right|^2}{R_z^2}\right), \tag{1}$$

$$\rho_{xj} = \exp\left(\frac{-\left|r_{xj}\right|^2}{R^2}\right)\exp\left(\frac{-\left|z_{xj}\right|^2}{R_z^2}\right), \tag{2}$$

where ρ_{ij} (ρ_{xj}) is the background error correlation interpolated to two observation (grid point/observation) locations, r_{ij} (r_{xj}) and z_{ij} (z_{xj}) are the horizontal and vertical distances between observation (grid point/observation) pairs and R (R_z) is a scaling parameter that determines the horizontal (vertical) background error correlation length scale.

Optimal interpolation (OI), three-dimensional variational (3DVAR), and Bratseth solutions were obtained from the sample of 500 sets of observations and background fields using the methods outlined by Kalnay (2003) and Matrix Laboratory (MATLAB) software. The background error correlations were defined by Eqs. (1) and (2) for the Bratseth method and a similar equation defined at gridpoint pairs was used for the OI and 3DVAR analyses. The horizontal and vertical correlation length scales were set to 75 km and 375 m respectively in part to reflect the

gross similarities in the background errors between the Salt Lake and Rush Valleys and the rapid changes in correlation with elevation. The ratio, σ, of observation error variance to forecast error variance was set to 0.1 to test the difficult situation when the analysis is intended to be constrained closely by the observations.

For each of the 500 analyses, one of the ten observations was withheld randomly in order to estimate the analysis skill by comparing the truth at the omitted location to the various analysis solutions. As summarized in Table 1, the analysis errors for the solutions with $R = 75$ km are identical and reflect a 14% improvement relative to the background error. Of course, if the actual background error correlation matrix defined from the entire sample of background fields is used, then the OI and 3DVAR averaged solutions equal truth (not shown). Further, an ensemble Kalman filter approach that provides a reasonable estimate of the background error correlation matrix in this case would be able to provide better analyses than the solutions shown here.

Since the sample averages of the OI, 3DVAR, and Bratseth analyses are identical, they are shown and labelled in Fig. 3a as a single line (75 km). Because the observation errors are specified in this case to be much smaller than the background errors, the analyses trend towards the observations and generally provide reasonable solutions. As shown in Fig. 3b, the analysis errors relative to the specified truth are substantially smaller than those of the background, especially in the centers of the Rush and Salt Lake Valleys.

However, systematic differences between the sample average solutions with $R = 75$ km and truth are evident in Fig. 3a. First, the magnitudes of the observation corrections (differences between the observation and background values at a specific location) are quite different from one side of the range to the other. Second, the horizontal and vertical length scales of the background error correlation are sufficiently large to allow the large negative observation corrections in the

center of the Rush Valley to influence the analysis in the Salt Lake Valley as is evident near 60 km where the analysis is too cool when compared to both the nearby observations and background field. Third, the large horizontal and vertical length scales allow smaller negative observation corrections in the Salt Lake Valley to influence the analysis in the Rush Valley as is evident near 25 km where the analysis is too warm compared to the local observations. Finally, the large negative corrections in the Rush Valley are given significant weight on the Salt Lake Valley benches while the positive observation corrections on those benches affect the analysis in the Rush Valley. The resulting analysis in the Salt Lake (Rush) Valley tends to be colder (warmer) than the truth. As shown in Fig. 3b, the analysis errors are particularly large over the western (eastern) bench of the Salt Lake (Rush) Valley.

The Bratseth solution converges to the OI/3DVAR solutions when the observation correction vectors on two successive passes are nearly the same (Daley 1991; Kalnay 2003). As shown in Fig. 4, 100 iterations were necessary to ensure that the Bratseth solutions converged completely to the same solutions as OI and 3DVAR. Pedder (1993) suggests that the rate at which the root mean square (RMS) differences decrease between successive observation correction vectors can be used to define a practical convergence limit to reduce computational costs. As a general rule, most applications of the Bratseth method have used a total number of 10 or fewer iterations (Seaman 1988; Franke 1988; Carr et al. 1996; Lazarus et al. 2002; Xue et al. 2003). To further assess the sensitivity of the Bratseth method to the number of iterations, the Bratseth analysis at the gridpoint locations was computed after each iteration. As shown in the inset frame of Fig. 4, a smaller number of iterations than that required for complete convergence can be justified since the RMS errors of the Bratseth solutions relative to truth approach the OI and 3DVAR errors (0.39°C) after roughly 10 iterations.

To mitigate the systematic differences in the objective analyses shown in Fig. 3, a smaller correlation length scale could be used. Analyses were obtained from another 500 member sample of observations and background fields with R set to 25 km and R_z unchanged. All three solutions had the same errors averaged over the 500 member sample as shown in Table 1 and the improvement relative to the background field increased from 14% to 30%. As evident in Fig. 3a, the smaller correlation length scale leads to a closer fit near the observations. However, the analyses are degraded in other locations, particularly along the western bench of the Salt Lake Valley (centered at 52 km), because the observation increments available on the eastern bench of the Valley no longer receive sufficient weight and the closest observation differs substantially in elevation. It should be recognized that the density of observations used in this example is higher than that for many parts of the western United States such that use of small correlation length scales leads to analyses in many parts of the West that are close to the background field.

As an alternative to reducing the background error correlation length scale throughout the analysis domain, we suggest reducing locally the background error correlation between locations that are separated by significant topography. An intervening terrain term (ITT) is introduced into Eqs. (1) and (2) to reduce the background error correlation where observations are located on the other side of a mountain range as follows

$$\rho_{ij}{}' \;=\; \rho_{ij}\exp\!\left(\frac{-\left|a_{ij}\right|^{2}}{R_{B}^{2}}\right),\tag{3}$$

$$\rho_{xj}{}' \;=\; \rho_{xj}\exp\!\left(\frac{-\left|a_{xj}\right|^{2}}{R_{B}^{2}}\right),\tag{4}$$

where a_{ij} (a_{xj}) is the magnitude of the terrain blockage between an observation/observation (grid point/observation) pair and R_B is the intervening terrain scale factor. The ITT is calculated by subtracting the height of the observation (z_j) or grid point (z_x) that is located at a higher elevation from the maximum height of the intervening terrain (z_t) (see Fig. 5). As a_{ij} or a_{xj} increase, the correlation between the background errors at the two locations decreases for a given R_B.

To evaluate the influence of the ITT, analyses were generated from the same 500 member samples of observations and background fields using the Bratseth method and Eqs. (3) and (4) with R set to 75 km and 25 km. The intervening terrain scale factor (R_B) was set to 2000 m, which implies that for a 500 m obstacle between two points, the correlation is reduced by only 23%. As shown in Table 1, the analysis error is reduced by 32% compared to the background field when the background error correlation length is set to 75 km and the ITT is used. Note that in this example, no additional analysis skill is gained by using the intervening terrain term when the value of the background error correlation length scale is less than or equal to width of the Oquirrh Mountains (i.e. $R = 25$ km).

As shown in Fig. 3, inclusion of the ITT eliminates some of the systematic errors that arise from the difference in observation corrections in the two valleys: the west bench of the Salt Lake Valley is significantly warmer while the east bench of the Rush Valley is colder. Note that the large biases of the background field can not be completely overcome in the center of the Rush Valley or on the western slope of the Salt Lake Valley, but the Bratseth approach with the ITT has the smallest errors in those locations of any of the various solutions. In addition, the Bratseth solution with the ITT converges faster than when it is omitted (Fig. 4) and the RMS errors of the Bratseth solution with ITT drop rapidly to a smaller value (0.28°C) than those obtained from the OI, 3DVAR or Bratseth solutions without the ITT.

Additional experiments were conducted to test the ITT. For example, during strongly forced situations it is unreasonable to expect that large observational differences will preferentially occur across mountain ranges; rather, the analysis should be dominated by the timing and position of mesoscale and synoptic features. To test this behavior, the radiation inversion was replaced by a case where temperature decreases with elevation and a strong cold front (cold to the west and warm to the east) was located randomly within the domain of Fig. 2. As was expected, little difference was found between the solutions with or without the ITT.

The sensitivity of the analysis to the ITT relative to the other tunable parameters has also been evaluated. A number of studies have shown that reducing the horizontal length scale used to define the background error correlation matrix (or decreasing the ratio of the observation to background error variance) hampers the convergence of the Bratseth solution to the best linear unbiased estimate of the truth (Pedder 1993; Ioannidou and Pedder 1999). For example, the Bratseth solution with the ITT did not completely converge to the OI/3DVAR solutions when the horizontal scale was reduced from 75 to 25 km even though there was no practical difference between the various solutions as evident from Table 1. If the observation to background error variance ratio (σ) is increased to 1.0, then the Bratseth analysis without the ITT converges after only 20 passes (not shown). As will be discussed in section 5, Franke (1988), Seaman (1988), Pedder (1993) and Ioannidou and Pedder (1999) also found that convergence of the Bratseth solutions to the best linear unbiased estimate can be impeded and it is possible to have solutions diverge away from the best estimate if the parameters used to define the background error correlation are improperly specified. The resulting solutions suffer from severe overfitting of the analysis to the observations.

3. ADAS

At the University of Utah, a modified version of ADAS is used to generate analyses of surface meteorological variables over the western United States for a variety of applications (Lazarus et al. 2002). ADAS typically incorporates over 2,000 surface weather observations each hour from MesoWest (Horel et al. 2002). Those observations, collected from over a hundred different agencies and firms, are spaced irregularly in the horizontal and are located at different terrain elevations in the vertical; some regions have relatively high data density (e.g., northern Utah, southern Nevada, San Francisco Bay region), while others do not (e.g., northeastern Arizona).

Significant changes have been made to the Utah ADAS code used to derive analyses of surface variables since the description provided by Lazarus et al. (2002). The background field used for the analyses has been updated from the 40-km to the 20-km version of the Rapid Update Cycle (RUC; Benjamin et al. 2004a). The domain was changed to a section of the Lambert Conformal projection grid 211 utilized by the National Digital Forecast Database (NDFD; Glahn and Ruth 2003) and the analysis is now performed on the 5-km NDFD terrain field. Currently, ADAS surface analyses are generated for temperature, relative humidity, pressure, and wind over the western United States in near real-time at 5-km horizontal resolutions every hour.

The methodology used to obtain the Bratseth analysis has been changed to that described by Daley (1991) and Kalnay (2003). The approach described by Bratseth (1986) that was followed in the original University of Oklahoma ADAS code solves separate equations during each iteration for the analysis at the observation and gridpoint locations. However, only the corrections at the observation locations need to be determined each iteration and the analysis at the gridpoints can be determined once after the final iteration. This change significantly reduces the computer time required to complete an analysis. In addition, since only objective analyses of surface vari-

ables are desired in our work, all of the code required to handle upper air, radar, and satellite observations has been removed from our most recent version of ADAS. This significantly reduces the memory required to perform the analysis.

Following the approach used by previous investigators (e.g., Lönnberg and Hollingsworth 1986), we have attempted to estimate appropriate horizontal (R) and vertical (R_z) scale factors by comparing RUC analyses during the 2003-2004 winter season to all available MesoWest observations. This work has been inconclusive especially since it is difficult to extract simultaneously the horizontal and vertical scales from the background error covariance matrix. Although the length scales for the case study in the next section have been fixed to 75 km horizontally and 375 m vertically, it should be noted that the ability to reduce the background error correlation scale as a function of iteration is a useful characteristic of the Bratseth analysis that is not possible with OI/3DVAR analyses (Bratseth 1986). Hence, different spatial scales likely to be present in the background error covariance matrix can be captured to some extent. For example, it allows the background field at most grid points to be adjusted by at least a few observations on the initial pass and the analysis to conform more closely to local observations in regions where the local data density is higher on later passes.

The intervening terrain scale factor (R_B) that restricts the influence of observation corrections through terrain has been set to 2000 m in order to limit the adjustments to major terrain features. For each observation/observation or observation/grid point pair, the terrain is searched along the most direct grid point route between the two points for the highest grid point elevation. Sensitivity tests showed that the amount of computation time added by the terrain searching was negligible.

4. Case Study

The effect of the ITT is now illustrated for ADAS analyses completed over the entire western United States. The terrain at 5-km resolution within a limited subdomain over northern Utah is shown in Fig. 1. As mentioned in Section 2, synoptic periods when nocturnal radiation inversions are present, are a difficult analysis problem, especially for surface temperature. A case study is presented for 1300 UTC 10 April 2003 during which strong radiation inversions were present in northern Utah with inverted surface temperature profiles within most basins (i.e., cold pools near the valley floors and warmer temperatures on adjacent slopes).

As mentioned earlier, it is possible to select combinations of the tunable parameters (R, R_z, R_B, and σ) that impede the convergence of the Bratseth solutions to the best linear unbiased estimation of the unknown truth. This was not apparent in our previous work when the specified observation to background error ratio was small ($\sigma = 0.06$ in this case) because only four iterations with a decreasing correlation length scale were used (Lazarus et al. 2002). For example, Fig. 6 shows the change in the observation corrections of the ADAS Bratseth solutions as a function of iteration for two different error ratios. If the observations are presumed to be nearly perfect (e.g., observational error equal to 6% of the background value) then the differences over the entire analysis domain between the two successive observation correction vectors remain large even after 100 passes. These large differences persist because of the difficulty to fit closely the analysis to the observations and leads to overfitting, i.e. unrealistic values in data void regions. However, when the observations and background errors are assumed to be equal ($\sigma = 1.0$), then the analyses converge and the solution using the ITT converges slightly faster (Fig. 6).

Because of the computational cost of using a large number of iterations to reach convergence, we have attempted to estimate the "computationally optimal" iteration after which no sig-

nificant change to the solution is likely to result. Our arbitrary definition of this threshold, based on the analytic case and a number of sensitivity tests with ADAS analyses, is the iteration after which the difference between successive correction vectors is less than 20% of the initial difference between the corrections on passes 1 and 2. For the analytic example in section 2, this threshold is reached after 8 iterations for the Bratseth solution with ITT, which on the basis of the RMS errors, meets conservatively our criterion that further iteration yields little additional benefit (Fig. 4). Using this rule of thumb suggests for this case that 20 passes are required to insure convergence if the ITT is used and 23 passes are required if it is not (Fig. 6). For example, the RMS difference between the observations and the analysis with the ITT after 20 passes is 2.98°C, which is identical to that after 100 passes, while it is 3.00°C if the ITT is omitted. The largest differences between the observations and the analyses in this case are found over northern Utah where radiation inversions were present and the data density is high, which leads to sharp changes in temperature over small distances.

The temperature observed at nearly all of the available stations in northern Utah is shown on three of the panels of Fig. 7 (a few stations have been omitted for clarity). A close inspection of the surface observations indicates that temperatures on the slopes (west slope and east bench) of the Salt Lake Valley are about 3°C higher than that observed on the valley floor. Temperatures in the Rush Valley were as much as 16°C colder than those in the Salt Lake Valley with inverted temperature profiles evident as well (e.g., -5°C in the northwest part of the Rush Valley to 12°C on its east bench).

Although the 20-km RUC background field interpolated to the 5-km grid does capture the general sense of warmer temperatures over the Great Salt Lake compared to that in the valleys to the southeast, it does not reflect the mesoscale temperature structure between and within the Salt

Lake, Rush and Tooele Valleys (Fig. 7a). For example, the background temperature within the Salt Lake Valley decreases with increasing elevation up the slopes while the background temperature in the Rush Valley lies between 6-8°C in comparison to the observed temperature range from -5 to 12°C.

As shown in Fig. 7b, the ADAS analysis using the background error correlations defined by Eqs. (1) and (2), resolves many of the mesoscale features in surface temperature, including the colder temperature values in the Rush Valley. However, the cold temperature observations in the Rush Valley contribute to large negative corrections elsewhere, including the southwestern corner of the Salt Lake Valley. The cooling, which results in analysis values between 4-7°C, occurs despite nearby observations on the order of 11-13°C and background temperatures ranging from 7-10°C (see Fig. 7b).

The ADAS analysis using the background error correlations defined by Eqs. (3) and (4) are shown in Fig. 7c. The coldest temperatures are now confined largely to the Rush Valley while the temperature has increased along the west slope of the Salt Lake Valley. Because of the sharp temperature gradients present over short distances, differences between the analysis and observations remain large in some locations. For example, this 5-km analysis can not capture the observed decrease in the temperature from 9°C at the top of the ridge between the Tooele and Rush Valleys to -1°C in a gap 4 km to the east referred to as the Stockton Bar.

The details of the underlying terrain field and value of R_B control how the analysis changes as a result of the ITT. For example, the influence of the ITT on the analysis in the northern Rush Valley and southern Tooele Valley is strongly tied to the scale of the terrain. The actual intervening terrain between these two valleys is 500 m. However, the analysis intervening terrain is only 200 m, which results in a temperature analysis in the southern Tooele Valley (northern

Rush Valley) that is colder (warmer) than that observed. A smaller value of R_B drives the analysis closer to the observations in these two valleys, but also contributes to overfitting elsewhere (not shown).

The differences between the ADAS solutions with and without the ITT are typically within a few degrees of one another (Fig. 7d) and demonstrate how the ITT restricts the influence of temperature corrections laterally through the terrain. Since the analysis relaxes back towards the warm background field in data void regions, the temperature has increased in the northern Skull Valley and other regions to the west of the Great Salt Lake. In addition, negative corrections from the cold observations in the Rush Valley are no longer able to propagate laterally resulting in positive differences where locally higher temperatures are observed such as the southern end of the Salt Lake Valley, to the north of Utah Lake, and to the southwest of the Stansbury Mountains. The opposite effect can be seen in the Rush Valley since the positive observation corrections or smaller negative corrections in the Salt Lake Valley receive less weight.

The differences between the analyses with and without the ITT are also evident in the cross-section along line segment AB in Fig. 7d shown in Fig. 8. Similar to the results of the analytic case shown in Fig. 3, the analyzed temperature has decreased in the Rush Valley by almost 1°C when the ITT is used while it has increased more than 1°C along the west slope of the Salt Lake Valley.

5. Discussion

Considerable research has demonstrated that analysis approaches that estimate directly the spatial relationships between background errors are superior to those that specify them a priori (Kalnay 2003). Nonetheless, there are many current applications that require economical analyses

of surface fields for which it is necessary to specify, as best as possible, the background error correlation matrix in an objective analysis system. The complex structure within this matrix is likely to be poorly defined if the correlations are assumed to be independent of location and large over distances that span mountain ranges.

A modification to the specification of the background error correlation matrix has been presented such that the analysis innovations are reduced when the locations of the observations and grid points are separated by major mountain ranges. The sensitivity of the analysis to this intervening terrain term has been demonstrated using an analytic example and a case study of cold pools in basins. In addition to providing an improved analysis compared to when it is omitted, this term speeds convergence of the Bratseth iterative method to the best linear unbiased estimation of the truth. Following Daley (1991) and Kalnay (2003), the Bratseth iterative approach as originally coded in ADAS has been made more efficient by completing the analysis at the gridpoints after the final iteration only.

The improved efficiency of the modified ADAS code makes it possible to continue until a reasonable approximation to the best linear unbiased estimate is reached. Following Pedder (1993), the decrease in the RMS difference between the observation corrections on successive passes can be used to define when this approximation is reached. We recommend that the common practice to use a fixed number of iterations for the Bratseth method should be avoided as convergence will depend upon the synoptic situation and distribution of available data.

The effect of the intervening terrain term on the analysis depends upon the local terrain and local data density more than the synoptic setting. The intervening terrain term will have a larger effect in regions such as the Great Basin characterized by narrow ranges and broad valleys. The analysis in data rich regions will trend towards the local observations while the analysis in

data voids will trend towards the background field. Hence, the analysis with the intervening terrain term, which is constrained more closely by local observations, will be superior to one without the term in data rich regions during all synoptic situations. In regions where observations are sparse, the background field remains the best choice during strongly-forced synoptic situations since corrections to the analysis based upon distant observations may introduce errors. For example, observation corrections within the pre-frontal environment would be inappropriate to apply to the post-frontal environment. However, the intervening terrain term degrades to some extent the analysis in data voids during weakly-forced synoptic situations such as the case presented in Fig. 7. Since the positive bias of the background field in this instance is grossly similar in all of the valleys, limiting the influence of distant observations degrades the analysis, for example, in the northern end of the Skull Valley. Our approach is a conservative one: constrain the analysis as much as possible to agree with local observations and, in their absence, adhere more closely to the background.

As discussed by Franke (1988), Seaman (1988), Pedder (1993) and Ioannidou and Pedder (1999), a disconcerting aspect of the Bratseth solution is that it is relatively easy to choose combinations of the horizontal (R) and vertical (R_z) background error correlation length scales, ratio of observation to background error variance (σ), and intervening terrain scale factor (R_B) that over the first few iterations appear to speed convergence yet eventually slow convergence or (after 20 or so iterations) lead to divergence, i.e., the RMS difference between the observation corrections on successive passes begins to increase. We have found that resulting solutions tend to suffer from severe overfitting of the analysis to the observations with unrealistic analyzed values in data void regions. The parameters chosen by Lazarus et al. (2002) and applied to surface analyses of tem-

perature over the western United States exhibited these characteristics when solutions were obtained after 20 or more iterations, especially on the periphery of data rich regions.

The tendency for the Bratseth analysis or other best linear unbiased estimation to overfit the observations is straightforward to diagnose and avoid. We recommend that enough iterations be completed to confirm that the solution is converging towards the optimal solution for the set of parameters used to specify the background error correlation matrix. As the horizontal background error correlation length scale (R) is decreased in Eq. (1), the analysis will be constrained more closely in data rich regions to fit the observations. In mountainous regions where the observations can vary significantly over short distances (e.g., Fig. 7), tight constraints to match the observations will lead to overfitting in adjacent data void areas. Each of the other tunable parameters can be viewed as simply modifying the local horizontal background error correlation length scale, e.g., the contribution from the vertical term arising from differences in the elevation of the 2 points is equivalent to a local (anisotropic) reduction in R. In other words, the same error correlation could be obtained if the vertical term were omitted and a smaller R chosen. As R_z decreases, this reduction in R becomes more pronounced and the analysis will be constrained more closely to fit the observations locally. Similarly, as the intervening terrain scale factor (R_B) in Eq. (3) decreases, the local horizontal length scale decreases. For example, we found that reducing R_B to 500 m produced analyses that fit the observations closely but generated unrealistic analysis values in nearby data void regions. Finally, as the ratio of the observation error variance to the background error variance decreases, the effective horizontal background error correlation length scale decreases as well. Overrelaxation factors (Franke 1988; Seaman 1988) and decreasing length scales as a function of iteration (Bratseth 1986; Sashegyi et al. 1993) that initially speed convergence can also contribute to overfitting.

A more subtle aspect of the overfitting problem is the choice of the scale over which to average the observations in order to remove local observational differences (Bratseth 1986; Kalnay 2003). Generating such superobservations based solely upon horizontal proximity is not recommended in mountainous regions since the observations at different elevations can reflect significantly different weather. An example was given in the previous section where a 10°C temperature difference was observed between two stations separated vertically by 250 m and 4 km horizontally. We limit superobing to stations within 1 km horizontally and 100 m vertically of another station.

Additional local modifications to the background error correlation matrix can be imposed. For example, we have added to Eqs. (3) and (4) a term that decreases the weight of observational corrections across coastlines of major lakes and oceans. We intend to pursue incorporating flow-dependent terms that would improve consistency between the wind and other fields. We also will continue identifying seasonal, diurnal, and synoptic dependencies of the background error correlations as a function of location. For example, our preliminary work suggests that the specification of the errors in terms of Gaussian weights (Eq. (1)) decreases the background correlations too abruptly with distance. We also intend to improve estimates of the errors inherent in the surface observations obtained from the various sources available from MesoWest.

data made available by the governmental agencies, commercial firms, and educational institutions

participating in MesoWest.

References

Benjamin, S. G., and N. L. Seaman, 1985: A simple scheme for objective analysis in curved flow. *Mon. Wea. Rev.*, **113**, 1184-1198.

-----, G. A. Grell, J. M. Brown, T. G. Smirnova, and R. Bleck, 2004a: Mesoscale weather prediction with the RUC hybrid isentropic terrain-following coordinate model. *Mon. Wea. Rev.*, **132**, 473-494.

-----, and Coauthors, 2004b: An Hourly Assimilation-Forecast Cycle: The RUC, *Mon. Wea. Rev.*, **132**, 495-518.

Bratseth, A. M., 1986: Statistical interpolation by means of successive corrections. *Tellus*, **38A**, 439-447.

Brewster, K. A., 1996: Application of a Bratseth analysis scheme including Doppler radar data. *Preprints, 15th Conf. on Wea. Analysis and Forecasting*, Norfolk, VA, Amer. Meteor. Soc., 92-95.

Carr, F. H., J. M. Krause, and K. Brewster, 1996: Application of the Bratseth scheme to high-resolution analyses in inhomogeneous data regimes. *Preprints, 15th Conf. on Wea. Analysis and Forecasting*, Norfolk, VA, Amer. Meteor. Soc., 231-234.

Daley, R., 1991: *Atmospheric data analysis*. Cambridge University Press, 457 pp.

Dee, D. P., and A. M. da Silva, 1998: Data assimilation in the presence of forecast bias. *Quart. J. Roy. Met. Soc.*, **124**, 269-295.

Deng, X., and R. Stull, 2004: A mesoscale analysis method for surface potential temperature in mountainous and coastal terrain. Submitted to *Mon. Wea. Rev.*

Doran, J. C., J. D. Fast, and J. D. Horel, 2002: The VTMX 2000 campaign. *Bull. Amer. Meteor. Soc.*, **83**, 537-551.

Endlich, R. M., and L. Mancuso, 1968: Objective analysis of environmental conditions associated with severe thunderstorms and tornadoes. *Mon. Wea. Rev.*, **96**, 342-350.

Franke, R., 1988: Statistical interpolation by iteration. *Mon. Wea. Rev.*, **116**, 961-963.

Glahn, H. R., and D. P. Ruth, 2003: The new digital forecast database of the National Weather Service. *Bull. Amer. Meteor. Soc.*, **84**, 195-201.

Hessler, G., 1984: Experiments with statistical objective analysis techniques for representing a coastal surface temperature field. *Bound.-Layer Meteor.*, **28**, 375-389.

Horel, J., and Coauthors, 2002: Mesowest: Cooperative mesonets in the western United States. *Bull. Amer. Meteor. Soc.*, **83**, 211-226.

Ioannidou, L., and M. A. Pedder, 1999: Three-dimensional applications of a successive corrections analysis scheme to mesoscale observations. *Mon. Wea. Rev.*, **127**, 236-251.

Kalnay, E., 2003: *Atmospheric Modeling, Data Assimilation and Predictability*. Cambridge University Press, 341 pp.

Lanzinger, A., and R. Steinacker, 1990: A fine mesh analysis scheme designed for mountainous terrain. *Meteor. Atmos. Phys.*, **43**, 213-219.

Lazarus, S. M., C. M. Ciliberti, J. D. Horel, and K. A. Brewster, 2002: Near-real-time applications of a mesoscale analysis system to complex terrain. *Wea. Forecasting*, **17**, 971-1000.

Lönnberg, P. and A. Hollingsworth, 1986: The statistical structure of short-range forecast errors as determined from radiosonde data. Part II: The covariance of height and wind errors. *Tellus* **38A**, 137-161.

Miller, P. A., and S. G. Benjamin, 1992: A system for the hourly assimilation of surface observations in mountainous and flat terrain. *Mon. Wea. Rev.*, **120**, 2342-2359.

Otte, T. L., N. L. Seaman and D. R. Stauffer, 2001: A heuristic study of the importance of aniso-
tropic error distributions in data assimilation. *Mon. Wea. Rev.*, **129**, 766-783.

Pedder, M. A., 1993: Interpolation and filtering of spatial observations using successive correc-
tions and Gaussian filters. *Mon. Wea. Rev.*, **121**, 2889-2902.

Sasaki, Y., 1971: A theoretical interpretation of anisotropically weighted smoothing on the basis
of numerical variational analysis. *Mon. Wea. Rev.*, **99**, 698-707.

Sashegyi, K. D., D. E. Harms, R. V. Madala, and S. Raman, 1993: Application of the Bratseth
scheme for the analysis of GALE data using a mesoscale model. *Mon. Wea. Rev.*, **121**, 2331-
2350.

Seaman, R. S., 1988: Some real tests of the interpolation accuracy of Bratseth's successive correc-
tion method. *Tellus*, **40A**, 173-176.

Smith, R., and Coauthors, 1997: Local and remote effects of mountains on weather: Research
needs and opportunities. *Bull. Amer. Meteor. Soc.*, **78**, 877-892.

Thiebaux, H. J., 1976: Anisotropic correlation functions for objective analysis. *Mon. Wea. Rev.*,
104, 994-1002.

-----, 1977: Extending estimation accuracy with anisotropic interpolation. *Mon. Wea. Rev.*, **105**, 691-699.

Xue, M., K. K. Droegemeier, and V. Wong, 2000: The Advanced Regional Prediction System (ARPS) - A multiscale nonhydrostatic atmospheric simulation and prediction model. Part I: Model dynamics and verification. *Meteor. Atmos. Phys.*, **75**, 161-193.

-----, and Coauthors, 2001: The Advanced Regional Prediction System (ARPS) - A multiscale nonhydrostatic atmospheric simulation and prediction tool. Part II: Model physics and applications. *Meteor. Atmos. Phys.*, **76**, 143-165.

-----, D. Wang, J. Gao, K. Brewster, and K. K. Droegemeier, 2003: The Advanced Regional Prediction System (ARPS), storm-scale numerical weather prediction and data assimilation. *Meteor. Atmos. Phys.,* **82**, 139-170.
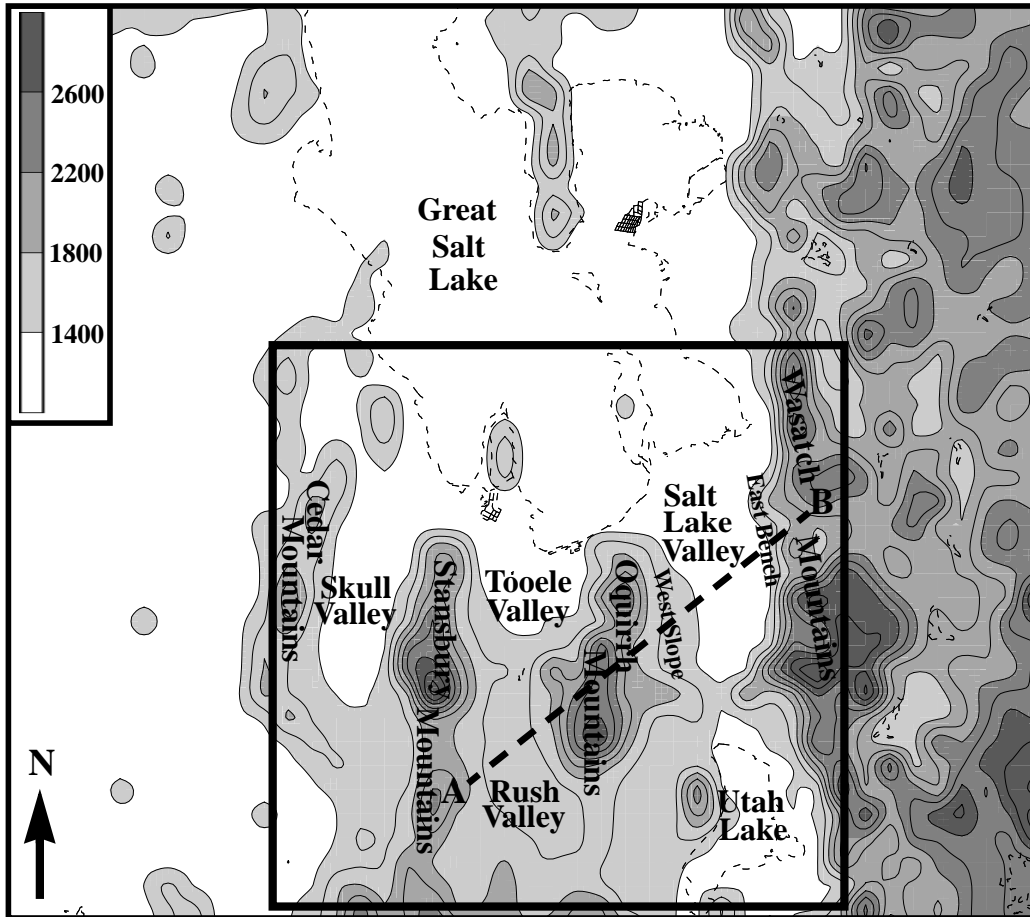
Figure Captions

Figure 1: Surface terrain (m, shaded according to scale, contoured every 200 m) and lakes (dashed black lines) for the Wasatch Front at 5-km resolution. The black box denotes the subdomain examined later in Fig. 7 and dashed line AB denotes the surface cross section shown later in Figs. 2, 3 and 8.

Figure 2: Specified true temperature profile, observation locations (shaded circles), sample average of observations (open boxes), sample mean of background fields, and idealized terrain along dashed line AB in Fig. 1.

Figure 3: a) Specified true temperature profile, sample average of observations (open boxes), and sample means of background and objective analyses. b) Root mean square errors derived from the 500 member sample for the background and objective analyses. See text for further details.

Figure 4: RMS difference in temperature corrections as a function of iteration for Bratseth solutions with and without intervening terrain term (ITT). Root mean square errors (RMS) of Bratseth solutions with and without ITT as a function of iteration (inset).

Figure 5: Schematic of analysis grid points (filled circles) and observations (open circles). The height of the intervening terrain for an observation/observation pair (a_{ij}) and grid point - observation pair (a_{xj}) is shown.

Figure 6: RMS difference in ADAS temperature corrections as a function of iteration with ITT (solid line) and without ITT (dashed line) when the observation to background error correlation ratio equals 1.0 and with ITT (dashed-dot line) when the observation to background error correlation ratio equals 0.06.

Figure 7: Wasatch Front region surface temperature observations (°C) and (a) RUC, (b) ADAS and (c) ADAS with ITT analyses of temperature (°C) for 1300 UTC 10 April 2003. (d) Difference between ADAS analyses with and without ITT (panel c minus panel b). Terrain and lakes are denoted by solid and dashed lines, respectively. The surface cross section shown later in Fig. 8 is denoted by dashed line AB in (d).

Figure 8: Difference between ADAS analyses of temperature with and without ITT at 1300 UTC 10 April 2003 (°C; dashed line) along 5-km terrain cross section (heavy solid line) AB in Fig. 7d.

Table 1: Analysis error (°C) at observation locations (see text for details).

	$R = 75$ km	$R = 25$ km
Background	1.01	1.01
Optimal Interpolation	0.87	0.71
3-D Variational	0.87	0.71
Bratseth	0.87	0.71
Bratseth ITT	0.69	0.71

Figure 1: Surface terrain (m, shaded according to scale, contoured every 200 m) and lakes (dashed black lines) for the Wasatch Front at 5-km resolution. The black box denotes the subdomain examined later in Fig. 7 and dashed line AB denotes the surface cross section shown later in Figs. 2, 3 and 8.

Figure 2: Specified true temperature profile, observation locations (shaded circles), sample average of observations (open boxes), sample mean of background fields, and idealized terrain along dashed line AB in Fig. 1.

Figure 3: a) Specified true temperature profile, sample average of observations (open boxes), and sample means of background and objective analyses. b) Root mean square errors derived from the 500 member sample for the background and objective analyses. See text for further details.

Figure 4: RMS difference in temperature corrections as a function of iteration for Bratseth solutions with and without intervening terrain term (ITT). Root mean square errors (RMS) of Bratseth solutions with and without ITT as a function of iteration (inset).

Figure 5: Schematic of analysis grid points (filled circles) and observations (open circles). The height of the intervening terrain for an observation/observation pair (a_{ij}) and grid point/ observation pair (a_{xj}) is shown.
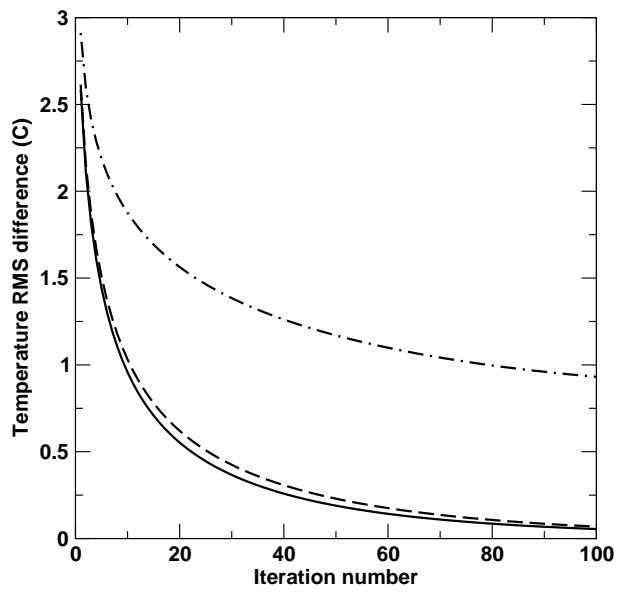
Figure 6: RMS difference in ADAS temperature corrections as a function of iteration with ITT (solid line) and without ITT (dashed line) when the observation to background error correlation ratio equals 1.0 and with ITT (dashed-dot line) when the observation to background error correlation ratio equals 0.06.
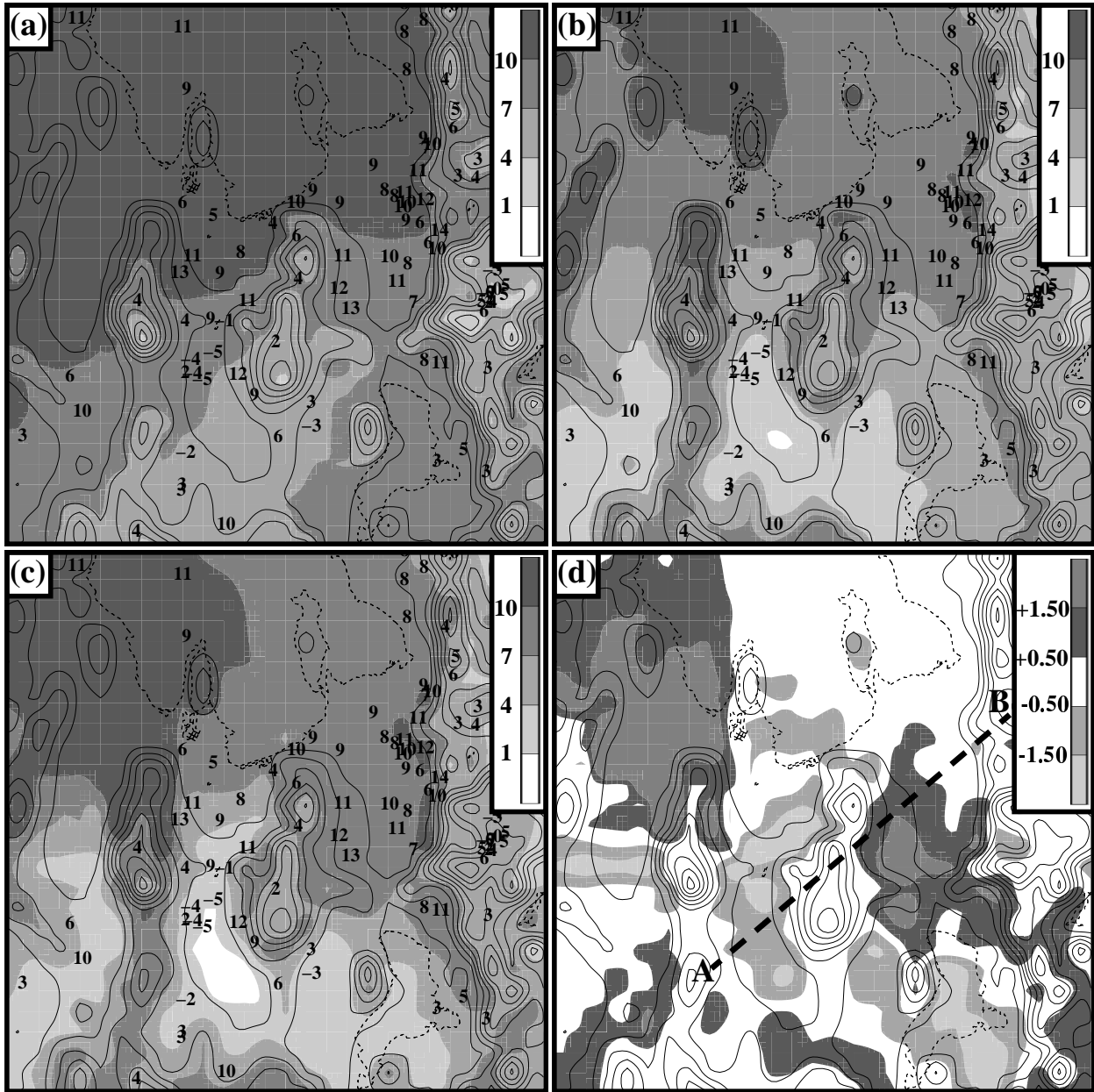
Figure 7: Wasatch Front region surface temperature observations (°C) and (a) RUC, (b) ADAS and (c) ADAS with ITT analyses of temperature (°C) for 1300 UTC 10 April 2003. (d) Difference between ADAS analyses with and without ITT (panel c minus panel b). Terrain and lakes are denoted by solid and dashed lines, respectively. The surface cross section shown later in Fig. 8 is denoted by dashed line AB in (d).
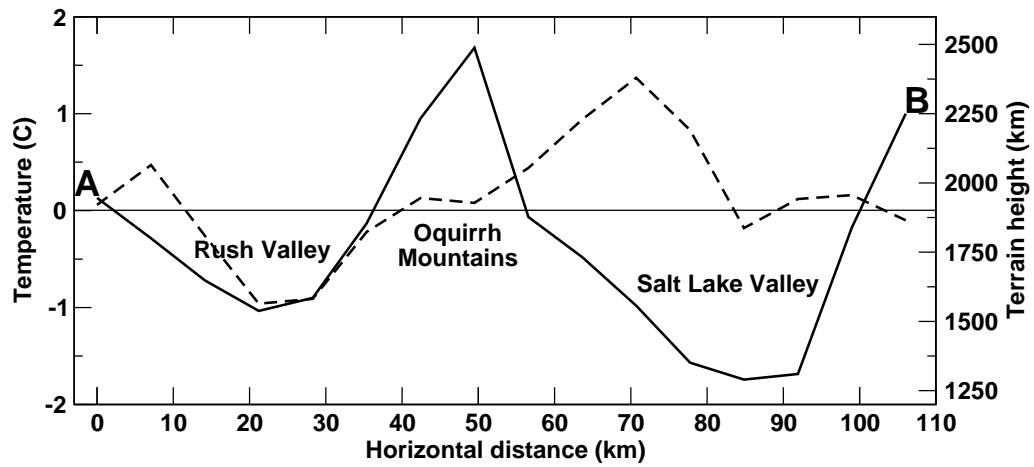
Figure 8: Difference between ADAS analyses of temperature with and without ITT at 1300 UTC 10 April 2003 (°C; dashed line) along 5-km terrain cross section (heavy solid line) AB in Fig. 7d.